PHILIPPINE ENGINEERING JOURNAL
PEJ 2021; Vol. 42, No. 1: 83-105

Air Change and Aerosol Evacuation Rates in a Two-Occupancy Room with Stand Fan for Forced Ventilation

Ken Bryan Fernandez, Jon Dewitt Dalisay and Menandro Berana
Department of Mechanical Engineering, College of Engineering,
University of the Philippines Diliman, Quezon City 1101 Philippines

Abstract — *In order to prevent the spread of COVID-19 through the airborne route for rooms without dedicated ventilation systems, stand fans can be used for forced ventilation through windows and doors. In this work, computational fluid dynamics (CFD) simulations of indoor airflow were performed using a CFD package to assess the effect of a single stand fan in terms of air change rate per hour (ACH) and evacuation rate of aerosols produced by two occupants. Four fan configurations were investigated in a room with one window and one door: (1) air intake near the door, (2) air exhaust near the door, (3) air intake near the window, and (4) air exhaust near the window. Additionally, two aerosol production cases were studied: (a) the occupant near the door solely produces the aerosols and (b) the occupant seated near the window solely produces the aerosols. Results show that all the configurations satisfy the DOLE guidelines for ACH of offices, and the intake configurations yielded about 2-4 times higher air change rates compared to the exhaust configurations. Remarkably, even though configuration 2 has the lowest air change rate per hour, it has the highest aerosol evacuation rate for case A. Although, this is undesirable for actual implementation since the door path is used by occupants going in and out of the room. Still, this study shows that the resulting air flow field and consequent aerosol transport is an important factor besides the air change rate when assessing the potential of spreading the disease.*

Keywords – Ventilation, Indoor Air Quality, Particle Dispersion, Computational Fluid Dynamics, COVID-19

I. INTRODUCTION

As of May 2021, around 155 million people have already been infected by COVID-19, and around 3.2 million died because of the virus. To prevent its spread, lockdowns, halting of production, and restriction of social gatherings were implemented in many countries. These actions negatively affected, and are still affecting the global economy [1]. Meanwhile, despite implementing the world's longest lockdown, the Philippines recorded around 1 million infections with 17 thousand deaths, and the running daily count of new cases is increasing yet again [1]. The country suffered 9.5% contraction in Gross Domestic Product (GDP) with almost 5 million Filipinos displaced in their jobs in 2020 [2].

Initially, COVID-19 was thought to be transmitted via respiratory droplets both through direct and indirect routes [3]. Direct transmission can occur when an infected person is in close proximity with a healthy one; the virus is spread through the droplets generated during coughing, sneezing, and even talking and breathing. On the other hand, an indirect route is manifested when the respiratory droplets generated by an infected individual fall on surfaces, a healthy person touches the contaminated surfaces, and then proceeds to touch their eyes, nose, or mouth where pathogens can enter. Accordingly, social distancing, use of face masks, and disinfection of surfaces and hands were recommended to deter virus transmission.

However, as the global pandemic ran its course, more and more evidences [4-6] suggest that COVID-19 is actually transmitted more effectively through the airborne route via aerosols (droplets with diameter of $\leq$ 5 micrometers) that remain in the air for 3 hours or longer depending on the ventilation [3]. These aerosols, being small in diameter and mass, can be transported by parcels of air, and can infect a healthy person if inhaled in sufficient amounts.

Since the airborne transmission of COVID-19 is very likely to happen inside closed rooms and buildings, it is necessary to review the ventilation strategies implemented in such indoor spaces [7-8]. One of the guiding principles in ventilation standards is the displacement of stale, possibly contaminated, air inside rooms through the introduction of fresh air from the outside. This strategy helps in preventing the increase of virus concentration inside rooms, and it is usually quantified using *air change rate*, or the measure of how many times the air inside a room is replaced by clean air outside for a given time interval. It is usually reported in hourly terms; for instance, it is recommended for hospital rooms to have 2-6 air changes per hour (ACH) [9]. Recently, the Department of Labor and Employment (DOLE) released a guideline of 6-12 ACH for offices and public transport [10]. Improvement of the air change rate is accomplished through opening windows and doors, adding dedicated inlet and exhaust ventilation systems, and adding fans for forced ventilation. In addition to air change rate, air flow fields inside rooms also need to be considered. The air flow field should not transport exhaled air of an infected occupant towards a healthy one, and there should be no flow patterns that allow the stagnation of air which can lead to aerosols settling in some parts of the room. Air flow fields can be improved through room layout modification and reorganization of ducting and fan placement. Both the air change rate and the air flow field dictate the transport of aerosols, from the moment they go out of the respiratory tract of an infected person until they go to every part of the room or to outside. Another strategy that can be implemented is the use of air filters and purifiers to remove or kill the virus.

To assess a ventilation system and strategy, experiments can be done to monitor the air flow and temperature profiles, and even the particle content profile, in different parts of a room, such as in the studies of Xue et al. [11], Liu et al. [12], and Lin et al. [13]. The success and usefulness of such experiments are highly dependent on the spatio-temporal resolution of the laser and imaging equipment in laser-based experiments, or the temperature and air flow sensors in sensor-based experiments. In indoor air flow experimental research, equipment costs can get quite prohibitive. This limitation gave way to the popularization of computational fluid dynamics (CFD) simulations for studying indoor air flow. Several CFD simulation studies, before and during the COVID-19 pandemic, were and are being performed to analyze the effectiveness of different ventilation strategies for different scenarios. Horan et al. [14] studied, using Ansys CFX software, the effects of external wind conditions, speed and direction, and the number of windows for the ACH of a naturally ventilated building. Variation of external conditions was shown to cause significant variation in ACH, while ACH was shown to be positively correlated to the number of windows. Lipinski et al. [15] studied, using Star-CCM software, the ventilation performance of two natural ventilation configurations, the *Windhive* and *Ventive Active*, for classroom set-up. Performance was assessed in terms of ACH, air flow profile, and CO_2 concentration profile. A constant release of 0.035 m^3/hour of CO_2 from each of the occupants was assumed in the study. They demonstrated a higher resulting ACH for the *Windhive* configuration (3.3) compared to *Ventive Active* (2.5). The *Windhive* configuration

also yielded favorable CO_2 ppm levels. Their study shows that natural ventilation is desirable since aerosols are not being pushed across the room. Abuhegazy et al. [16] investigated, using Ansys Fluent with a k-ϵ RNG turbulence model, the effects of particles size, aerosol source location, barriers, and windows in the aerosol transport inside a classroom. They found that around 24 – 50% of the particles smaller than 15 micrometers exit the system within 15 minutes. They also found that opening the windows increased the particle exit fraction by 38%. Borro et al. [17] performed coupled Eulerian-Lagrangian CFD simulations of a waiting room inside a hospital building. The particles are modeled with a Rosin-Rammler distribution. Their results show that the implemented HVAC system helps in the dilution of infected particles. However, it also helped in the transport of the infected particles across the room after a coughing event. Kabrein et al. [18] performed CFD simulations, using Ansys Fluent with a k-ϵ RNG turbulence model, to investigate the effect of air change rate to CO_2 concentrations in a room. They also performed subsequent experimental validation of the simulation results. A fixed flow rate of CO_2 from each of the occupants was assumed in the study. They found that CO_2 concentrations are high near breathing zones and low near the walls where air velocities are relatively low. The temperature, velocity, and CO_2 profiles generated were found to be in accordance with ASHRAE standards. Bhattacharya et al. [19] simulated the airflow inside a hospital room with an air-conditioning and aerosol-sanitizing system, using unsteady CFD with a k-ω SST turbulence model. Compared to the previous studies, the particles were aimed to reach every part of the room, since it is assumed that the viral particles are already killed using the sanitizer.

Until now, the University of the Philippines Diliman (UPD) is still delivering courses online in order to prevent the spread of disease. On the other hand, offices that are needed for processing urgent and important documents, e.g., the Budget Office and the Human Resources Development Office, have to continue their operation, which requires their staff to report physically to work. Upon official inspection, they are observed to follow protocols, e.g., face mask wearing and social distancing requirements. However, the offices only have air-conditioning systems for thermal comfort which is unsatisfactory from a ventilation standpoint. The installed systems allow the indoor circulation of air but do not promote air exchange with fresh outside air. Immediate strategies recommended were the opening of windows and the addition of stand fans for forced ventilation. The stand fans were also recommended to be placed near windows, and in some cases, near doors, so they can serve as inlet and/or exhaust devices, thus increasing air exchange rates. The current work aims to study, using 3D CFD, these immediate strategies in order to improve insight and provide more detailed recommendations. The specific objectives of the current work are as follows:

1. Determine, for a single room with 2 occupants, the improvement in air change rate due to the installation of a single stand fan under 4 configurations: (1) air intake near the door, (2) air exhaust near the door, (3) air intake near the window, and (4) air exhaust near the window.

2. Investigate, for a single room with 2 occupants, the resulting transport of aerosol exhaled by a single occupant, i.e., whether aerosols get evacuated from the room, deposited on surfaces, or stay airborne indoors.

II. METHODOLOGY

In this work, Ansys Fluent 19.2 was used for the three-dimensional (3D) CFD simulations. The k-ϵ realizable turbulence model was adopted, similar to previous studies of indoor air flow [20]–[23]. Although some studies showed the effectiveness of k-ϵ RNG turbulence model, the preliminary simulations we performed were not able to produce satisfactorily converged solutions, thus leading us to continue with k-ϵ realizable turbulence model. The pressure-based coupled scheme, which was compared with the SIMPLE scheme on section 2.3, was used as the solver. Least Squares Cell Based scheme for gradient was used for a balance of accuracy and computational time [24]. Furthermore, the second order scheme for pressure transport, and the second order upwind scheme for both momentum and turbulence transport were used to maximize accuracy for a mesh generally unaligned with the flow field. Lastly, the cut-cell method, a hexahedral dominant meshing technique, was used since preliminary simulations for the default linear and quadratic tetrahedral elements failed to produce converged solutions.

Since the focus of this study is the effect of the single stand fan for forced ventilation, the effects of external conditions, e.g., external air velocity and turbulence, were neglected. Additionally, the air-conditioning system was set to be turned-off as the opening of windows and doors may overload the system due to very high air infiltration load. The boundary conditions of the two openings, the door and the window, were set as 0 gauge pressure inlet and outlet. The choice of setting one as the inlet and the other as the outlet depends on the location and orientation of the single stand fan. For example, when dealing with the configuration with air intake near the door, the door is specified to be an inlet and the window is specified to be an outlet. Moreover, we emphasize that both pressure-specified boundary conditions allow backflow as it is an important consequence of not having the stand fan flush with either boundary. Lastly, a convergence criterion of 1×10^{-3} was set for all residuals.

The door and window mass flow rates of all the configurations were monitored and were used for the determination of air change rate per hour given by the equation

$$ACH = \frac{\dot{m}}{\rho_{fluid} V_{room}} \times 3600 \qquad (Eq. 1)$$

where

$\dot{m} = mass\ flow\ rate\ \left(\frac{kg}{s}\right)$,
$\rho = density\ of\ the\ fluid = 1.225\ \frac{kg}{m^3}$, and
$V_{room} = volume\ of\ the\ room\ (m^3)$.

Note that at steady-state, the mass flow rate going in is equal to the mass flow rate going out. Therefore, we can use either the door or window mass flow rate for this calculation, regardless of whichever is an inlet or an outlet.

2.1. Room Geometry, Layout, and Objects

The geometry and layout of an existing room ($6.731\ m \times 3.429\ m \times 2.690\ m$) in UPD with two openings, the door ($2.083\ m \times 0.889\ m$) and the window ($1.470\ m \times 1.170\ m$), was

used in the study. The approximate lay-out of the room is shown in Figure 1 and the simplified geometries of the sitting occupants, their work tables and computer monitors are shown in Figure 2.

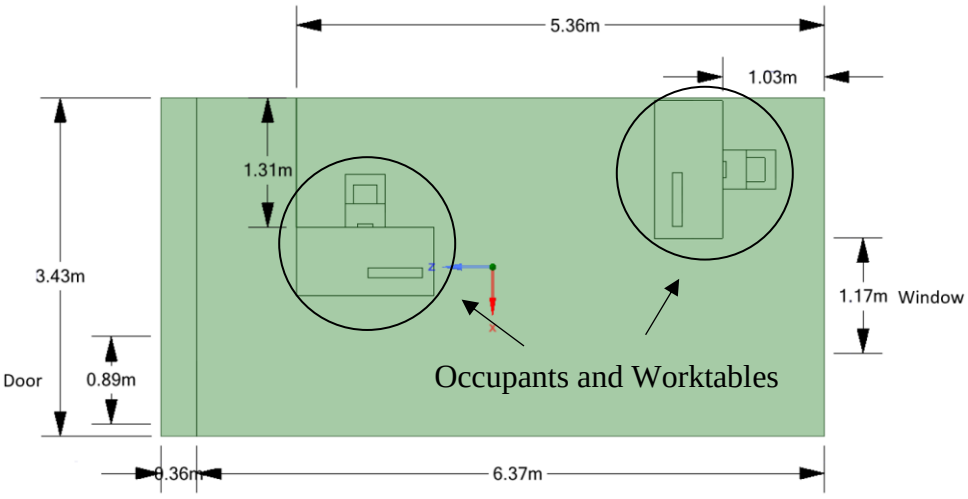

Figure 1: Room Lay-out

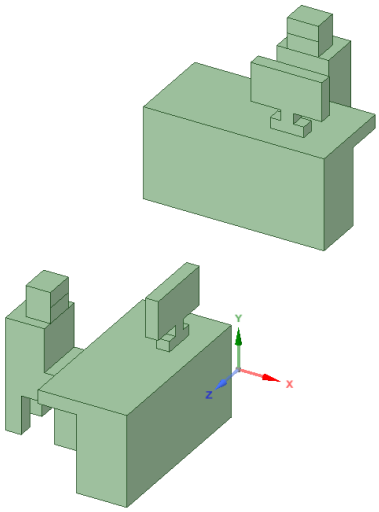

Figure 2: Simplified Occupants and Worktables

The front or back of the fan is assumed 1 foot ($\sim 0.30\ m$) away from the boundary and the distance from the front/back to blades is half of the thickness of the fan ($0.06\ m$). Thus, the fan internal boundary condition was placed $0.036\ m$ away from either at the center of the door or window. The four configurations: (1) air exhaust at the door (fan door exhaust, FDE), (2) air intake at the door (fan door intake, FDI), (3) air exhaust at the window, (fan window

exhaust, FWE) and (4) air intake at the window (fan window intake, FWI) are illustrated in Figure 3.

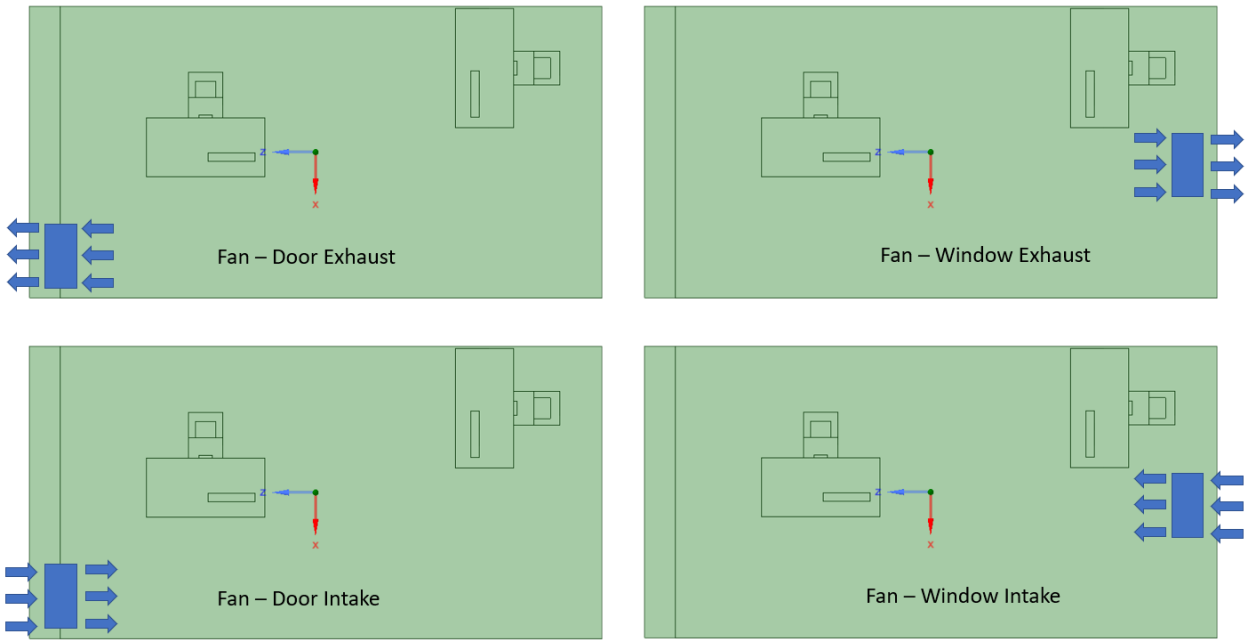

Figure 3: Fan Configurations

2.2. Modeling the Fan from Experiments

An infinitely thin surface internal boundary condition, one of the validated models of Krol et al. [25] in their study, was used to model the fan. In order to determine the boundary condition properties, actual dimensions were measured, and its performance was characterized.

(a) (b)

Figure 4: (a) Actual Fan (b) Pressure and Velocity Measurement Devices (Pasco Xplorer GLX)

The measured dimensions of the actual fan as shown Figure 4a are as follows: $0.41\ m$ total diameter, $0.10\ m$ hub diameter, and $0.13\ m$ fan thickness. These values are used to create a 3-D model of the fan in ANSYS Spaceclaim. The input for the boundary condition was a single pressure jump value, since the actual stand fan does not have an indicated fan curve and it is assumed to run at a single steady mass flow rate. This pressure jump is computed from experimental measurements of a fan operated at the highest speed; it is the average of measured pressure jumps at the points shown in Figure 4a. Table 1 shows the measurements and the final average value of 16.711 Pa.

Table 1: Measurement of Pressure Jumps

Delta Pressure (Pascal)	A	B	C	D	E
1	18.766	22.578	18.203	20.469	25.922
2	26.344	28.195	25.664	28.586	32.203
3	30.305	28.382	29.187	32.735	34.148
4	13.18	16.132	23.773	10.258	25.656
5	1.594	-0.219	6.492	3.094	-0.266
6	-2.179	0.015	2.711	-1.000	0.390
Average Per Line	14.668	15.847	17.672	15.690	19.676
Overall Delta Pressure	16.711				

The boundary condition allows for swirling, which is important in modeling the induced flow correctly. In order to characterize the swirl, CFD analyses of varying tangential velocity component were performed using a geometry with only a fan in a vacant 3-D space. From these analyses, we determined the tangential velocity component required to minimize the error with respect to experimental measurements. The radial velocity component of such stand fans is negligible [26-27] so it is set to $0\ \mathrm{m/s}$ in this study. The elements of the mesh are set to be hexahedral with a maximum element size of 50 mm. While first assuming that the tangential velocity component is negligible, gradient adaption was performed to enforce mesh independence: elements with velocity gradients $> 0.01\ m/s$ were successively refined until the average sum of squared velocity errors, between the previous and the current mesh, at a vertical line situated 30 cm away from front of the fan (Figure 5) goes < 0.01.

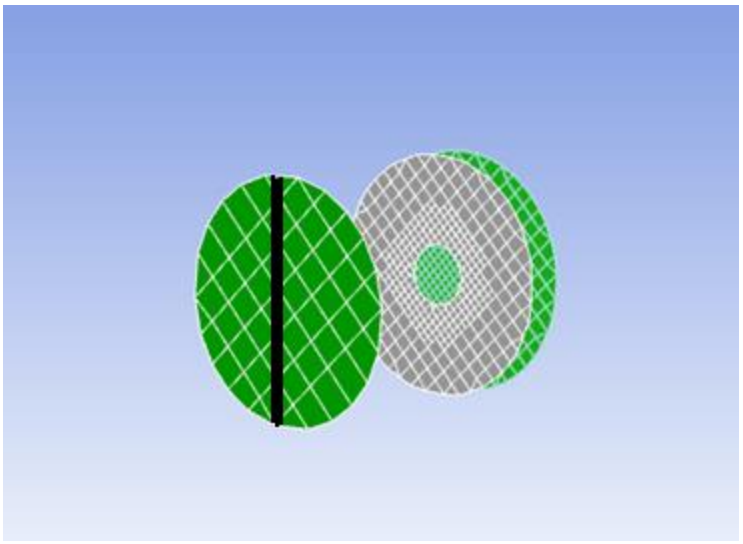

Figure 5: Vertical Line 30cm Away From Fan (Face A)

Table 2: Actual Velocity Measured at Face A

Position from the Ground (m)	Measured Velocity (m/s) (From Top to Bottom of Point A)
0.797	2.12 +/- 0.6
0.834	4.14 +/- 0.5
0.871	4.76 +/- 0.5
0.897	4.54 +/- 0.1
0.923	3.78 +/- 0.2
0.974	3.52 +/- 0.4
1.025	3.66 +/- 0.5
1.076	4.58 +/- 0.3
1.102	4.62 +/- 0.2
1.128	3.96 +/- 0.4
1.203	2.02 +/- 0.3

The axial velocities at Face A (Figure 5) were measured experimentally as listed in Table 2. Using the adapted mesh, the tangential velocity component was varied from 0 to $1\ \mathrm{m/s}$ at increments of $0.1\ \mathrm{m/s}$. The case with the minimum average sum of squared velocity errors

between the experiments and simulations can be identified from this parametric analysis, as seen in Figure 6. The resulting tangential velocity (0.6 m/s) is then used for this study.

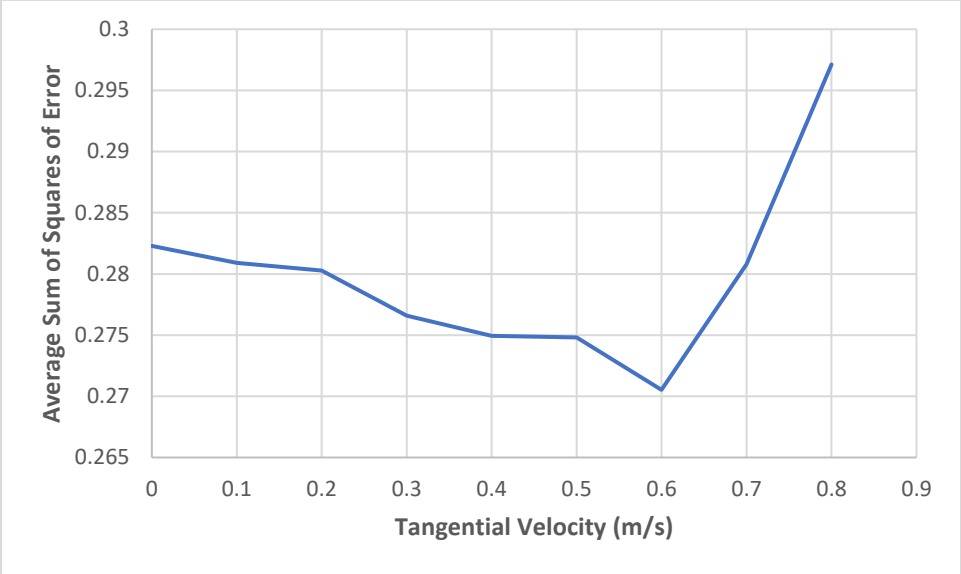

Figure 6: Average Sum of Squares of Error Versus Tangential Velocity (m/s)

2.3. Solver Choice and Mesh Dependence Studies

Preliminary steady-state simulations with global maximum element sizes of x mm (x elements), 50 mm (~350000 elements), 100 mm (70000 elements), and 200 mm (20000 elements), were performed for all fan configurations to determine the solver that will be used for the study, and ensure mesh independence. The comparison between two different solver algorithms are in Table 3. Although using different solvers (Coupled vs. SIMPLE) yielded close results, the Coupled solver was chosen since it produced converged solutions for all configurations and element numbers.

Table 3. Solver Versus Corresponding Mass Flow Rate Values

Mass Flow Rate (kg/s)								
	Fan Door Intake		Fan Door Exhaust		Fan Window Exhaust		Fan Window Intake	
Element Number	SIMPLE	Coupled	SIMPLE	Coupled	SIMPLE	Coupled	SIMPLE	Coupled
~350000	0.78149*	0.81715	0.21792	0.22106	0.28497	0.28635	0.63023	0.61221
~70000	0.79318*	0.75368	0.21959	0.22174	0.28642	0.29526	0.62562*	0.61725
~20000	0.64826*	0.70962	0.24278	0.22105	0.27586	0.29077	0.65744*	0.67551

**did not converge, values taken in 2000 iterations*

The mesh dependence study results using the Coupled solver is in Table 4. The mass flow rates at the door and window were compared with those of the finest mesh. Specifying a criterion of less than 5% error for mesh independence, we proceed with using approximately 70,000 elements for the rest of the study.

Table 4: Element Number Versus Corresponding Mass Flow Rate Values

	Fan Door Intake		Fan Door Exhaust		Fan Window Exhaust		Fan Window Intake	
Element Number	Mass Flow Rate (kg/s)	Percent Error	Mass Flow Rate (kg/s)	Percent Error	Mass Flow Rate (kg/s)	Percent Error	Mass Flow Rate (kg/s)	Percent Error
~1300000	0.78999	-	0.22468	-	0.28737	-	0.63673	-
~350000	0.81715	3.44	0.22106	1.60	0.28635	0.35	0.61221	3.85
~70000	0.75368	4.60	0.22174	1.30	0.29526	0.73	0.61725	3.06
~20000	0.70962	10.52	0.22105	1.61	0.29077	1.18	0.67551	6.09

2.4. Time Step Size Dependence Study for Transient Simulations

Reducing the convergence criterion for the residuals down to 1×10^{-4} produced oscillating residuals for steady-state simulations. We surmised that there is inevitable transient behavior in the system, so we decided to do transient simulations for the study. The Courant number, a non-dimensional number for time-integration schemes that should ideally have a value of ≤ 1 [28], was monitored. It is given by the equation

$$C = \Delta t \left(\frac{u}{\Delta x} + \frac{v}{\Delta y} + \frac{w}{\Delta z} \right) \qquad (Eq. 2)$$

where

$C =$ Courant number,
$u, v, w =$ flow velocities in m/s along the x, y, and z directions, respectively,
$\Delta t =$ time step size in seconds, and
$\Delta x, \Delta y, \Delta z =$ element sizes in meters along the x, y, and z directions, respectively.

For the simulations to have a maximum Courant number of less than 1, both the intake and exhaust configurations of fan near the door should have a time step of 0.0005 seconds, while it should be 0.00025 s for configurations of fan near the window. The transient simulations were also performed at time-steps of 0.005 s and 0.05 s for the door configurations, while 0.0025 s and 0.025 s for the window configurations. It can be seen in Figure 7 and Figure 8 that, even though the maximum Courant number exceeded the value of 1 for larger time steps, the mass flow rates approach similar steady-state behavior. This is possibly due to the Courant number being large only at small regions of the domain, and thus not affecting the overall behavior of the flow field very much. In order to decrease the computational expense, 0.05-s time steps are adopted for fan-near-the-door configurations, and 0.025-s time steps are adopted for fan-near-the-window configurations.

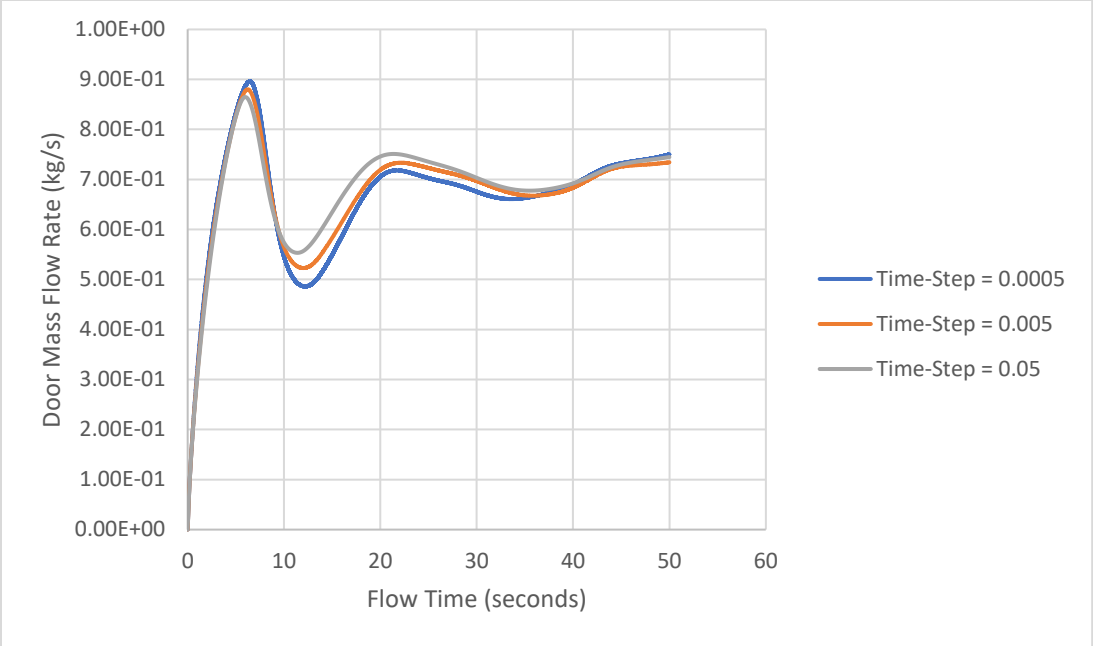

Figure 7: Time-Step Comparison (Fan Door Intake)

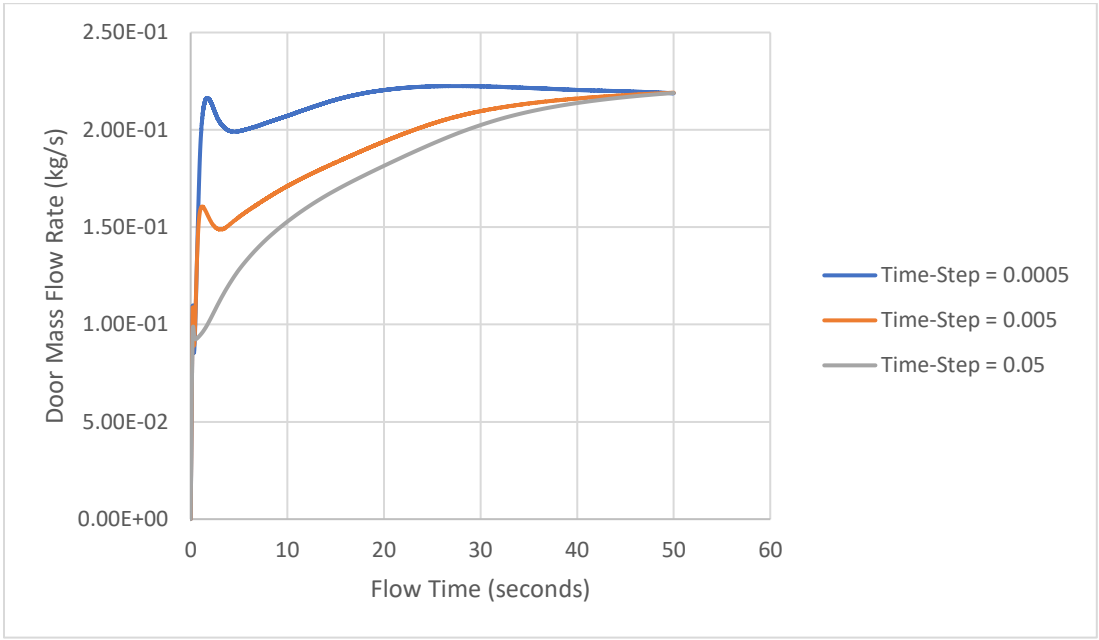

Figure 8: Time-Step Comparison (Fan Door Exhaust)

2.5. Discrete Phase Model

The discrete phase model used in the studies of Zhai et al. [29] and Li et al. [30] was used for particle tracking in this study. This Lagrangian model predicts the movement of the particle based on the integration of external forces due to the fluid phase [31]. In this work, the

Saffman lift, virtual mass, and pressure gradient forces were not included. For simplicity, a uniform particle diameter was set to be 0.26 microns, which is based on a study of mean diameters of human-generated aerosols [32]. The particle size limit is based on the use of surgical masks (these are used by occupants of the room being studied) which allow penetration of particles with aerodynamic diameters less than 5 microns [33-34]. Evaporation or growth rate of particles due to temperature and relative humidity was neglected. The particle velocity was set to be 4 m/s for normal breathing, and 15 m/s for coughing events [35]. The default stochastic tracking discrete random walk model was used to disperse the particles based on the instantaneous turbulence of the fluid phase. Lastly, the particle fate upon contact with the boundaries were summarized in the table below.

Table 5: Discrete Phase Model Boundary Condition

Boundary	Particle Fate
Door	Escape
Window	Escape
Floor and Walls	Trap
Occupants and Worktables' Surfaces except Mouth	Trap
Infected Occupant's Mouth	Reflect
Healthy Occupant's Mouth	Escape

The particles were continuously injected from an infected occupant's mouth starting from 60 seconds flow time. This starting point is when the mass flow rates at the door and window reach a steady-state value or oscillation. The simulations last until 240 seconds flow time. Breathing and coughing events were modeled through the variation of velocity coming from the infected occupant's mouth. It was assumed that the area of the mouth is 5% of the total area of the mask, thus, to estimate the particle velocity through the mask, continuity equation was used given by

$$(\rho_{air})(A_{mask})(V_{mask}) = (\rho_{air})(A_{mouth})(V_{mouth}) \qquad (Eq. 3)$$

where

$\rho_{air} = density\ of\ air\ in\ kg/m^3$
$A_{mask} = area\ of\ the\ mask\ in\ m^2$
$V_{mask} = velocity\ of\ the\ particle\ through\ the\ mask\ in\ m/s$
$A_{mouth} = area\ of\ the\ mouth\ in\ m^2$
$V_{mouth} = velocity\ of\ the\ particle\ from\ the\ mouth\ in\ m/s$

Figure 9 shows the assumed variation of the particle velocity through the mask in a 10-second interval. The healthy occupant is assumed to have 0 velocity boundary condition. The fate of each particles, whether escaped, trapped on the walls, or still circulating inside the room were recorded. The process was repeated for the case where the infected and healthy roles were switched.

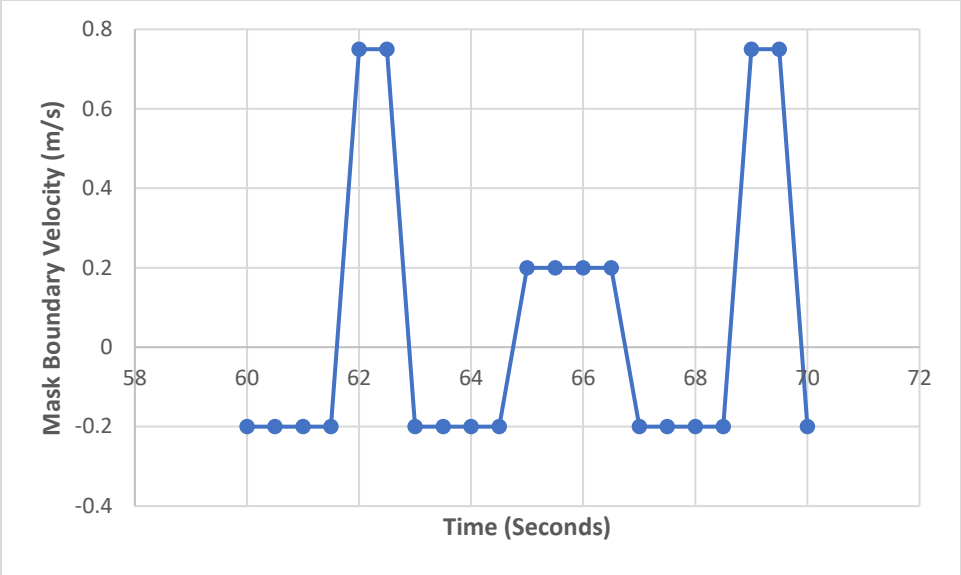

Figure 9: Infected Occupants Mask Velocity Versus Time

III. RESULTS AND DISCUSSION

3.1. Air Change Rates

Table 6: Air Changes Per Hour of the Four Configurations

	Air Changes Per Hour			
	FDE	FDI	FWE	FWI
Min	15.31	55.86	18.68	45.45
Max	16.67	61.47	20.68	53.30
Average	16.19	59.06	20.19	49.90

Shown in Table 6 are the values of air change rates for the four configurations. Note that because of flow oscillations, the ACH varies between minimum and maximum values. The fan intake configurations produced relatively higher rates, by about 2 to 4 times, compared to the fan exhaust configurations. The highest average value is 59.06 ACH for the fan door intake (FDI) configuration, followed by fan window intake (FWI) with 49.90 ACH, and the lowest average value is 16.19 ACH for the fan door exhaust (FDE), followed by fan window exhaust (FWE) with 20.19 ACH. This peculiar behavior can be explained by flow reversals at the boundary near the fan, when the fan is set to be an exhaust. This is illustrated for the FDE configuration in Figure 10. The low-pressure region at the back of the exhaust fan allows air to come in from the door. This decreases the weighted average of the mass flow rate at the door, thus decreasing the air change rate as well.

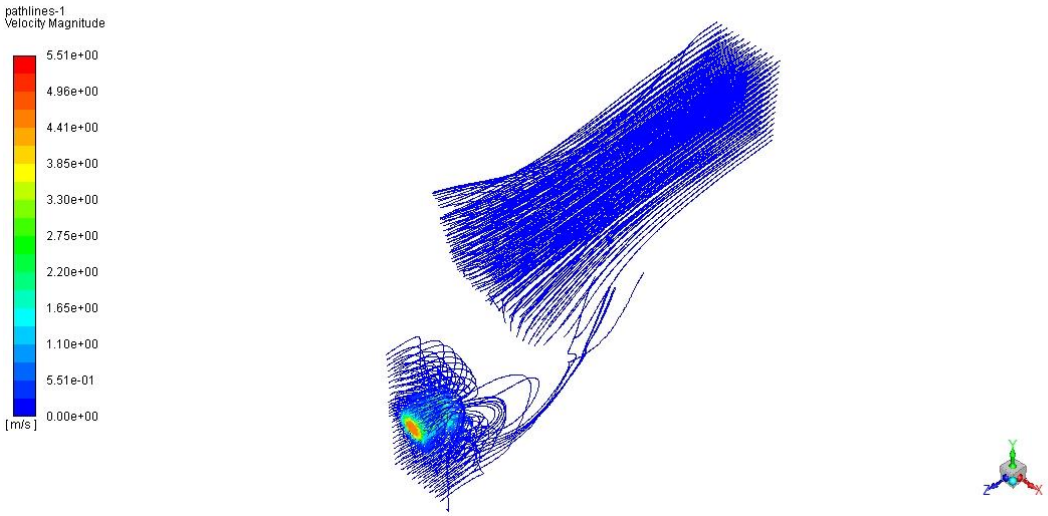

Figure 10: Path lines of FDE Configuration

3.2. Particle Transport

The fates of the aerosols coming from the infected occupant (man near the door for case A and man near the window for case B) are tabulated below. For case A, the configuration with the best evacuation rate is FDE, with 27.21% of the total particles generated exiting through the door. Additionally, no particle has reached the side of the healthy occupant for this configuration. On the other hand, the FWE configuration has the highest number of particles still circulating the domain which is 33.58%. For case B, the highest evacuation rate is seen in the FDI configuration with 10.54% of the total particle generated exiting through the window. On the other hand, FDE and FWE configurations have a high number of particles still circulating within the domain with values of 30.01% and 27.31%, respectively.

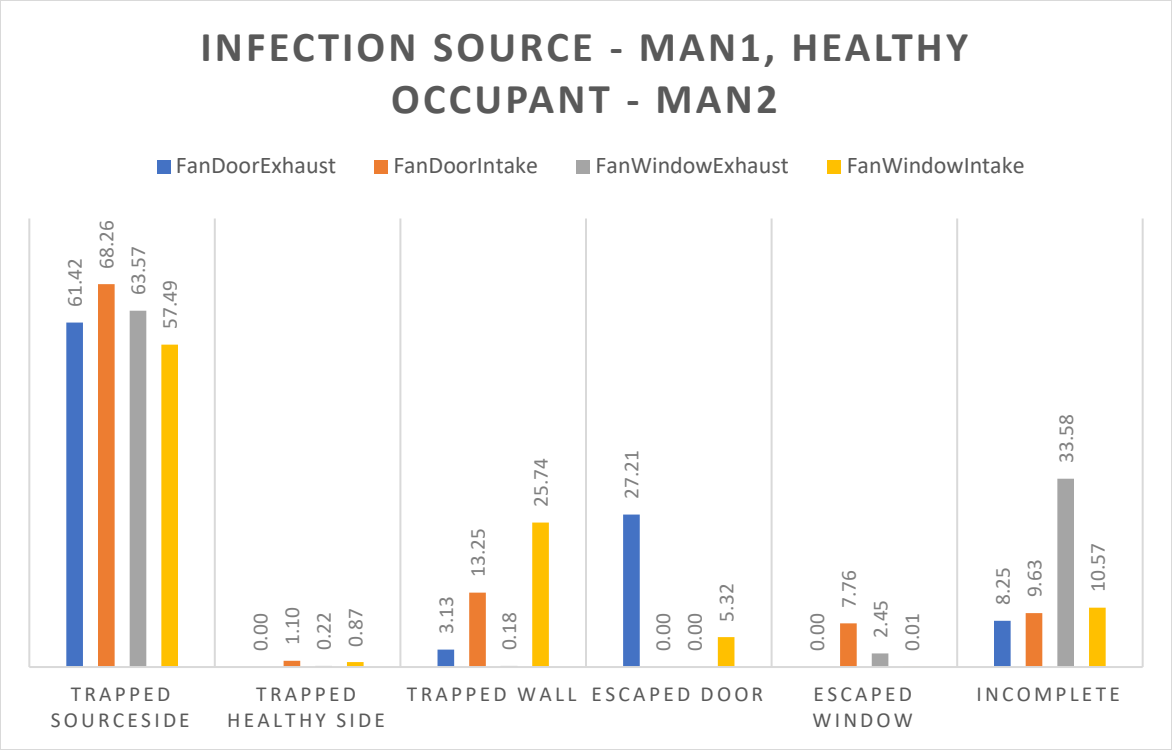

Figure 11: Particle Fate Case A

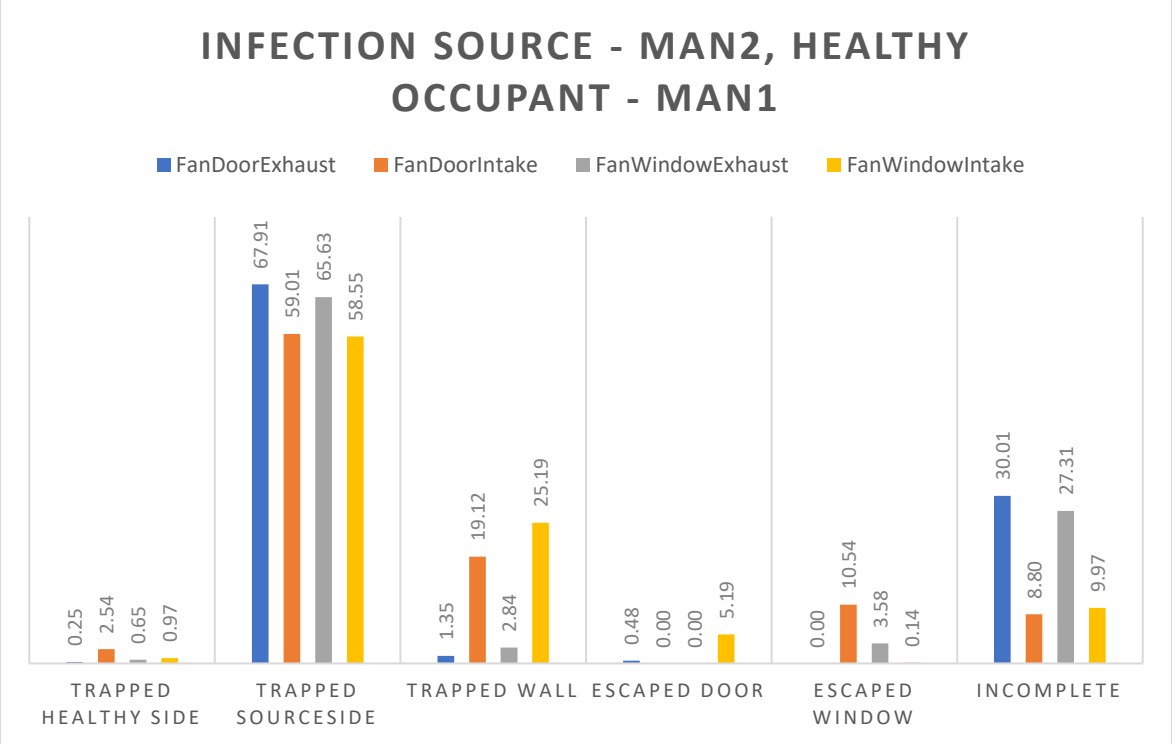

Figure 12: Particle Fate Case B

Case A under the FDE configuration having the most desirable result can be explained by looking at the air flow field in a horizontal plane created at the level of the infected occupant's mouth (Figure 13). After the breathing or coughing events, the resulting air flow field moves the particles directly towards the exhaust fan and then through the door. There are no nearby vortex structures that can bring the particles to other parts of the room. Furthermore, Figure 14 shows that almost all the particles at $t = 240$ s are near the door, i.e., the infected occupant's side, and no particles are present in the other side of the room.

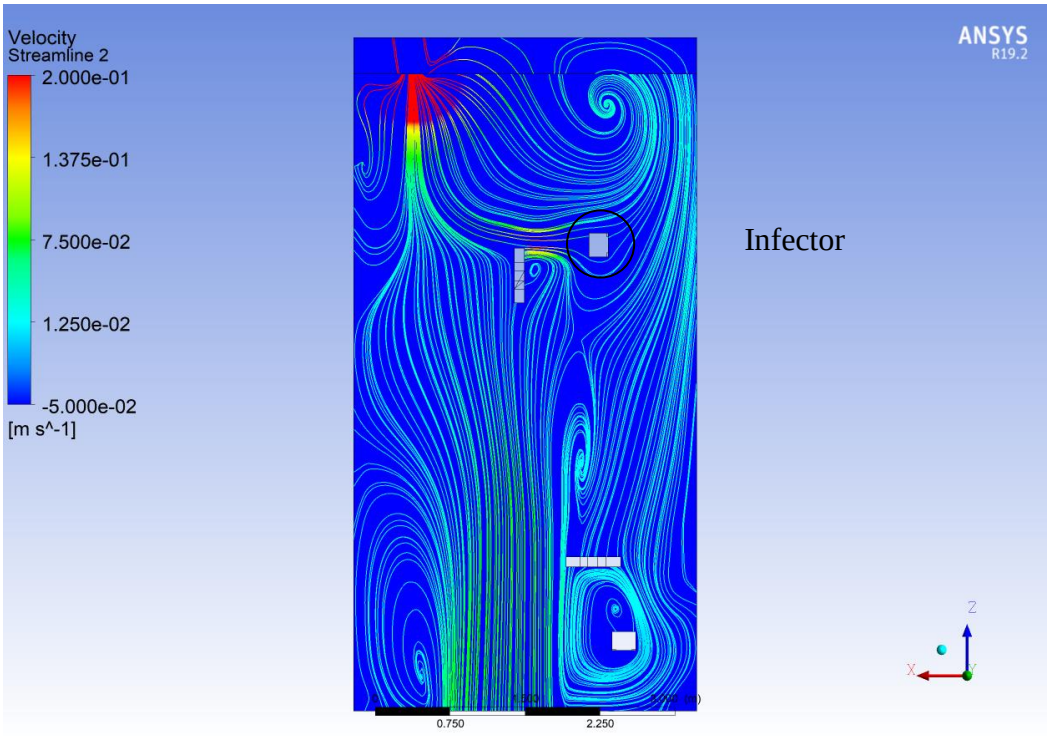

Figure 13: Flow Field FDE (Case A)

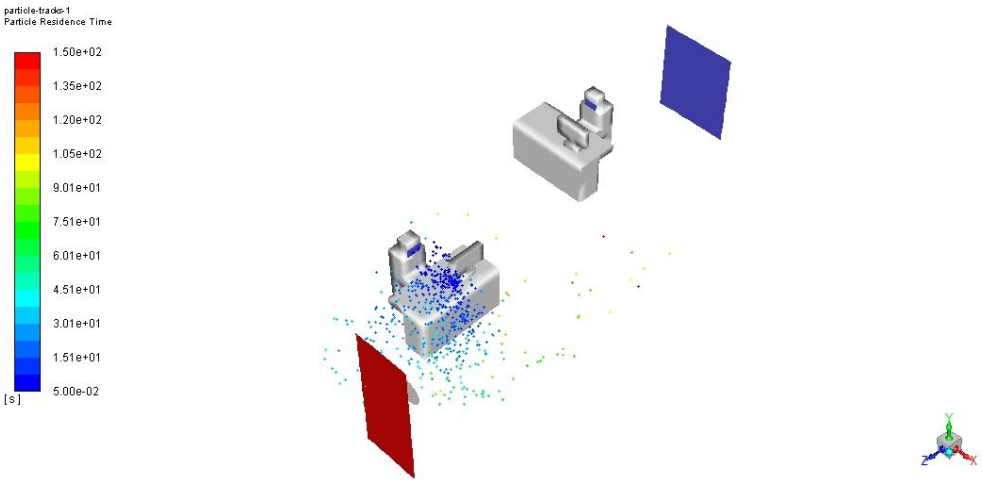

Figure 14: Particle Dispersion FDE (Case A)

The presence of incomplete particles, i.e., those still circulating within the domain, is undesirable since these particles can still be breathed in, or deposit on surfaces that can be touched, by the healthy occupant. The air flow fields of FWE configuration for cases A and B, with incomplete particles of 33.58% and 27.31%, respectively, both have a large vortex structure between the infected and healthy occupants. This is shown in Figure 15 and Figure 17. After coughing or breathing events, particles follow the streamlines leading to the aforementioned vortex structure. This led to the particles being circulated in the space between the occupants as shown in Figure 16 and Figure 18.

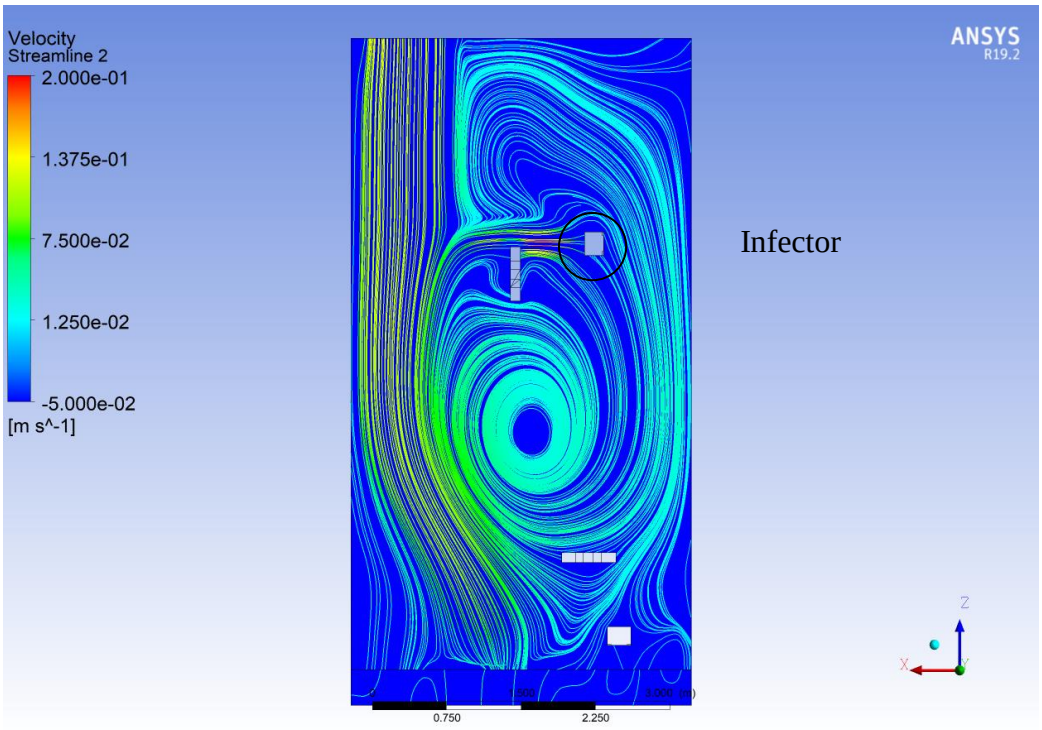

Figure 15: Flow Field FWE (Case A)

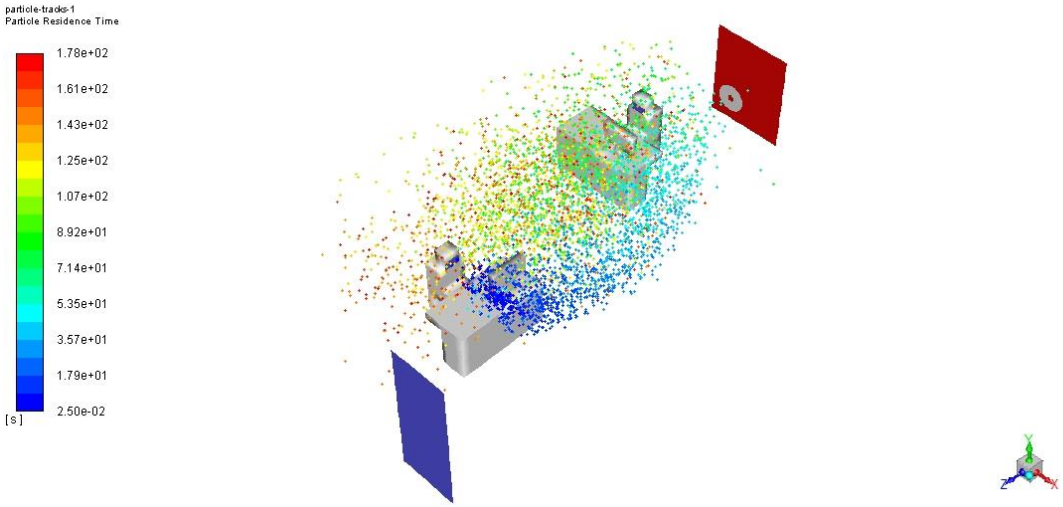

Figure 16: Particle Dispersion FWE (Case A)

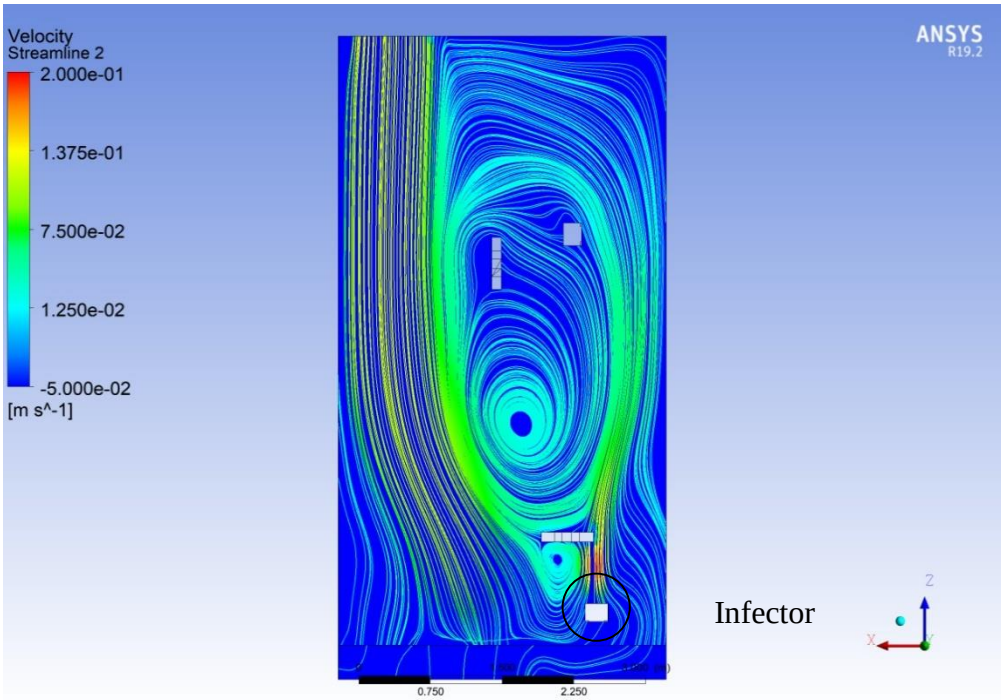

Figure 17: Flow Field FWE (Case B)

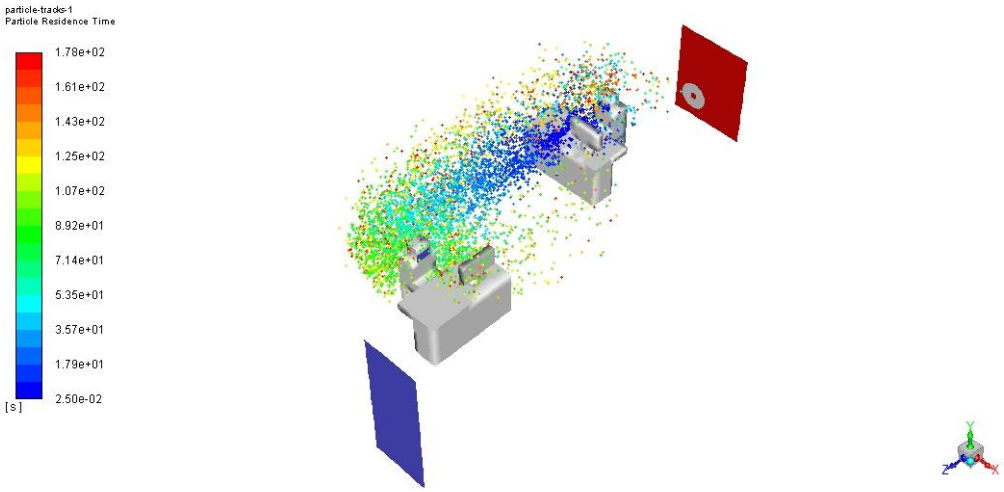

Figure 18: Particle Dispersion FWE (Case B)

On the other hand, case B of the FDE configuration with 30.01% incomplete particles has an isolated vortex structure near the infected occupant. This localizes the particles in the space near the infected occupant so only a small fraction is accessible by the healthy occupant.

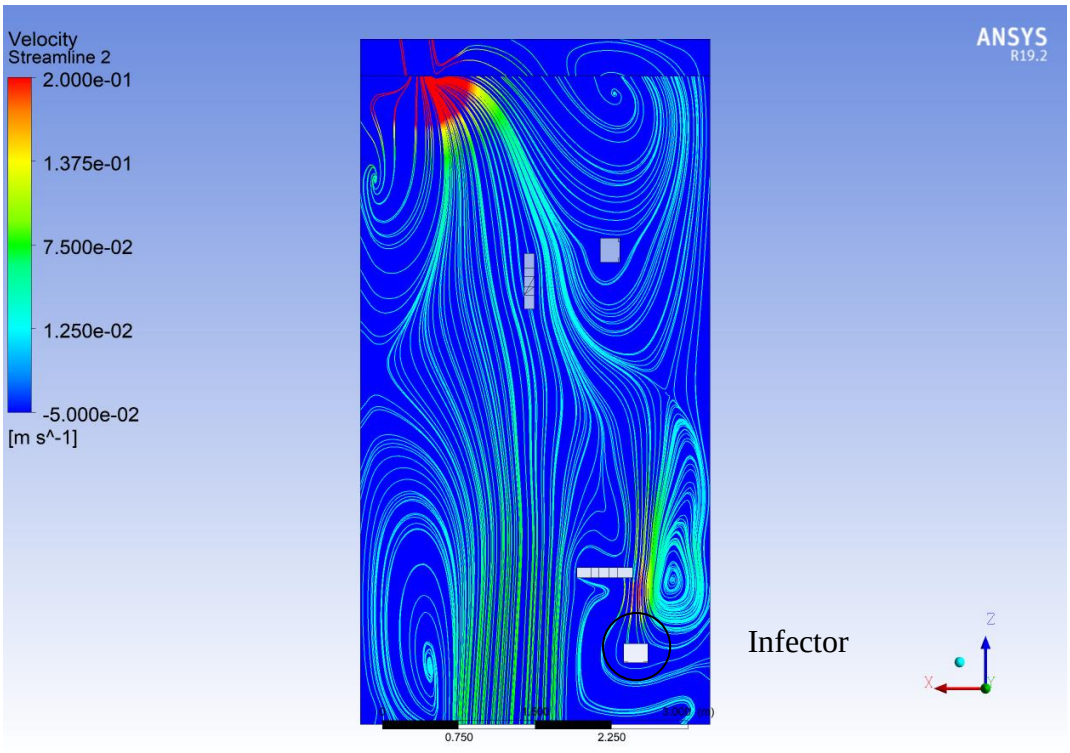

Figure 19: Flow Field FDE (Case B)

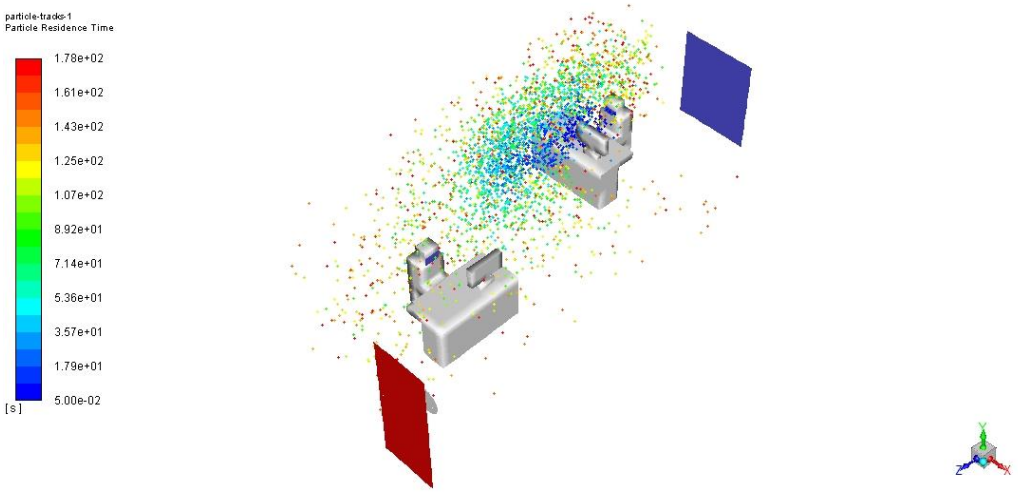

Figure 20: Particle Dispersion FDE (Case B)

3.3. Relationship Between Air Change Rate and Particle Transport

Even though the air change rate is a measure of how well the stale air inside the room is displaced by fresh clean air outside so higher magnitude is theoretically better, the current study shows that the configuration with the highest air change rate did not have the most desirable particle evacuation characteristics. The FDI configuration, with the highest average air change rate of 59.06, only has an evacuation percentage of 10.54% for case B. In stark

contrast, Case A of the FDE configuration, with the lowest average air change rate of 16.19, has an evacuation percentage of 27.21%. The important implication of the current study is that: the air flow field inside the room is a decisive factor in determining the fate of the aerosols inside a room, in addition to the air change rate. This supports the fact that the use of localized or personalized ventilation systems in restaurants and hospitals, although has a very minimal effect on the room air change rate, is very effective in evacuating particles in the room, whether they be contaminants or odor.

IV. CONCLUSION

A 3-D CFD study was performed to assess the effect of using a single stand fan for forced ventilation, in a single room with two occupants, to the air change rate and the particle transport. Results show that the intake configurations (49.90 and 59.06 ACH) produced higher values of air change rates compared to exhaust configurations (16.19 and 20.19 ACH). Additionally, case A of the fan-door-exhaust configuration resulted to the highest particle evacuation percentage (27.21% of generated particles) which is attributed to the resulting air flow field directing the aerosols from the infected occupant's mouth to the door exit. The current study shows that determining, and perhaps changing, the air flow field inside a room is an important factor besides increasing the air change rate, in terms of particle evacuation.

Even though case A of the fan-door-exhaust configuration resulted to the highest particle evacuation percentage, particle evacuation is primarily through the door. This is undesirable for actual implementation, since the door path is used by occupants going in and out of the room. Based on the study of air flow fields, a better recommendation would be to implement the fan-window-exhaust configuration and relocate the two occupants on opposite sides of the window. In this configuration, breathed and coughed aerosols will be sucked right away by the stand fan and deposited out the window where no other individuals will be present. This can be verified in the future by extending the configurations of the current study.

The current study is an isothermal analysis of the indoor environment. In reality, temperature gradients may affect not only the natural convection of indoor air, but also the growth or evaporation rate of airborne liquid particles. Non-isothermal analysis is recommended for future investigation. Moreover, forces due to auxiliary effects such as Saffman lift, virtual mass, and pressure gradient can be included in the discrete phase model for better prediction of particle dispersion.

The paper was also limited to certain configurations of stand fan position and direction. The effects of fan distance from the exit point, fan angle, exit area, and room layout on the flow field and particle transport can be studied in future work. Lastly, exploring the movements of the occupants in relation to the particle transport may be done in future work.

V. ACKNOWLEDGEMENT

The authors would like to thank the Post-ECQ Monitoring Committee of UP Diliman for giving the opportunity to do this research, and the reviewers for giving insightful comments and recommendations.

REFERENCES

[1] Worldmeters. 2021. COVID live update: 154,973,048 cases and 3,241,024 deaths from the Coronavirus. Retrieved from https://www.worldometers.info/coronavirus/ on 5 May 2021.

[2] Philippine News. 2021. Retrieved from https://philnews.ph/2021/02/04/dole-almost-5-million-filipino-employees-lost-jobs-pandemic/ on 5 May 2021.

[3] World Health Organization. 2020. Transmission of SARS-CoV-2: implications for infection prevention precautions. Retrieved from https://www.who.int/news-room/commentaries/detail/transmission-of-sars-cov-2-implications-for-infection-prevention-precautions on 5 May 2021.

[4] Jang S, Han SH, Rhee JY. 2020. Cluster of Coronavirus disease associated with fitness dance classes, South Korea. Emerging Infectious Diseases, 26(8): 1917-1920. doi: 10.3201/eid2608.200633.

[5] Kutter JS, Spronken MI, Fraaij PL, Fouchier RA, Herfst S. 2018. Transmission routes of respiratory viruses among humans. Current Opinion in Virology. 28(7):142-151. doi: 10.1016/j.coviro.2018.01.001.

[6] Hamner L, Dubbel P, Capron I, Ross A, Jordan A, Lee J, Lynn J, Ball A, Narwal S, Russell S, Patrick D, Leibrand H. High SARS-CoV-2 Attack rate following exposure at a choir practice. Morbidity and Mortality Weekly Report High. 69(19):606–610. Retrieved from: https://www.cdc.gov/mmwr/volumes/69/wr/mm6919e6.htm.

[7] United States Environmental Protection Agency. ND. Retrieved from https://www.epa.gov/coronavirus/indoor-air-homes-and-coronavirus-covid-19 on 5 May 2021.

[8] Kohanski MA, Lo LJ, Waring MS. 2020. Review of indoor aerosol generation, transport, and control in the context of COVID-19. Int. Forum Allergy Rhinol. 10(10):1173-1179. doi: 10.1002/alr.22661.

[9] [ASHRAE] American Society of Heating, Refrigerating and Air-Conditioning Engineers, Inc. (US). 2020. ASHRAE Position Document on Infectious Aerosols. Atlanta, Georgia.

[10] Department of Labor and Employment. 2021. Retrieved from https://www.dole.gov.ph/news/do-224-21-guidelines-on-ventilation-for-workplaces-and-public-transport-to-prevent-and-control-the-spread-of-covid-19/ on 17 May 2021.

[11] Xue K, Cao G, Liu M, Zhang Y, Pedersen C, Mathisen HM, Stenstad LI, Skogås JG. 2020. Experimental study on the effect of exhaust airflows on the surgical environment in an operating room with mixing ventilation. Journal of Building Engineering. 32:101837. doi: 10.1016/j.jobe.2020.101837.

[12] Liu X, Lv X, Peng Z, Shi C. 2019. Experimental study of airflow and pollutant dispersion in cross-ventilated multi-room buildings: effects of source location and ventilation path. Sustainable Cities and Society. 52:101822. doi: 10.1016/j.scs.2019.101822.

[13] Lin T, Lin KY, Omid Ali Zargar, Oscar Juina. 2020. An experimental study of the flow characteristics and velocity fields in an operating room with laminar airflow ventilation. Journal of Building Engineering. 29(1):1-9. doi: 10.1016/j.jobe.2020.101184.

[14] Horan JM, Finn DP. 2008. Sensitivity of air change rates in a naturally ventilated atrium space subject to variations in external wind speed and direction. Energy and Buildings. 40(8):1577–1585. doi: 10.1016/j.enbuild.2008.02.013.

[15] Lipinski T, Ahmad D, Serey N, Jouhara H. 2020. Review of ventilation strategies to reduce the risk of disease transmission in high occupancy buildings. International Journal of Thermofluids. 7-8:100045. doi: 10.1016/j.ijft.2020.100045.

[16] Abuhegazy M, Talaat K, Anderoglu O, Poroseva SV, Talaat K. 2020. Numerical investigation of aerosol transport in a classroom with relevance to COVID-19. Physic of Fluids. 32(10) doi:10.1063/5.0029118.

[17] Borro L, Mazzei L, Raponi M, Piscitelli P, Miani A, Secinaro A. 2021. The role of air conditioning in the diffusion of Sars-CoV-2 in indoor environments: a first computational fluid dynamic model, based on investigations performed at the Vatican State Children's hospital," Environmental Research.

193:110343. doi:10.1016/j.envres.2020.110343.
[18] Kabrein H, Hariri A, Leman AM, Yusof MZM, Afandi A. 2017. Experimental and CFD modelling for thermal comfort and CO2 concentration in office building. IOP Conf. Ser. Mater. Sci. Eng. 243(1). doi: 10.1088/1757-899X/243/1/012050.
[19] Bhattacharyya S, Dey K, Paul AR, Biswas R. 2020. A novel CFD analysis to minimize the spread of COVID-19 virus in hospital isolation room. Chaos, Solitons and Fractals. 139: 110294. doi: 10.1016/j.chaos.2020.110294.
[20] Sekhar C, Zheng L. 2018. Study of an integrated personalized ventilation and local fan-induced active chilled beam air conditioning system in hot and humid climate. Building Simulation. 11(4):787-801 doi: 10.1007/s12273-018-0438-8.
[21] Alotaibi S, Chakroun W, Habchi C, Ghali K, N Ghaddar. 2018. Effectiveness of contaminant confinement in office spaces equipped with ceiling personalized ventilation system. Building Simulation. 11(4):773–786. doi: 10.1007/s12273-018-0437-9.
[22] Habchi C, Ghali K, Ghaddar N, Chakroun W, Alotaibi S. 2016. Ceiling personalized ventilation combined with desk fans for reduced direct and indirect cross-contamination and efficient use of office space. Energy Conversation and Management. 111:158-173 doi: 10.1016/j.enconman.2015.12.067.
[23] El-Fil B, Ghaddar N, Ghali, K. 2016. Optimizing performance of ceiling-mounted personalized ventilation system assisted by chair fans: assessment of thermal comfort and indoor air quality. Science and Technology for the Built Environment. 22(4):412–430 doi: 10.1080/23744731.2016.1158072.
[24] Michalcová V, Kotrasová K. 2020. The numerical diffusion effect on the cfd simulation accuracy of velocity and temperature field for the application of sustainable architecture methodology. Sustainability. 12(23):1-18. doi: 10.3390/su122310173.
[25] Król A, Król M. 2018. Study on numerical modeling of jet fans. Tunnelling and Underground Space Technology. 73:222-235, 2018. doi: 10.1016/j.tust.2017.12.024.
[26] Hennissen J, Temmerman W, Berghmans J, Allaert K. 1997. Modelling of Axial Fans for Electronic Equipment. Thermal Management of Electronic Systems II. p. 309-318. doi: 10.1007/978-94-011-5506-9_30.
[27] Morris SC, Good JJ, Foss JF. 1998. Velocity measurements in the wake of an automotive cooling fan. Experimental Thermal and Fluid Science. 17(1-2):100-106. doi: 10.1016/S0894-1777(97)10054-1.
[28] Courant R, Friedrichs K, Lewy H. 1986. Über die partiellen Differenzengleichungen der mathematischen Physik. Kurt Otto Friedrichs. p. 53-95. doi: 10.1007/978-1-4612-5385-3_7.
[29] Zhai Z(J), Osborne AL. 2013. Simulation-based feasibility study of improved air conditioning systems for hospital operating room. Frontiers of Architectural Research. 2(4):468–475. doi: 10.1016/j.foar.2013.09.003.
[30] Li H, Zhong K, Zhai Z(J). 2020. Investigating the influences of ventilation on the fate of particles generated by patient and medical staff in operating room. Building and Environment. 180:1-11. doi: 10.1016/j.buildenv.2020.107038.
[31] ANSYS FLUENT 12.0 Theory Guide - 15.2.1 Equations of Motion for Particles. Retrieved from https://www.afs.enea.it/project/neptunius/docs/fluent/html/th/node241.htm#disp-thermophoretic-force on 10 June 2021.
[32] Pourdeyhimi B. 2020. Surgical mask particle filtration efficiency (PFE). Journal of Science and Medicine. 2(3):1-11. doi: 10.37714/josam.v2i4.50.
[33] Milton DK, Fabian MP, Cowling BJ, Grantham M L, McDevitt JJ. 2013. Influenza virus aerosols in human exhaled breath: particle size, culturability, and effect of surgical masks" PLoS Pathog. 9(3). doi: 10.1371/journal.ppat.1003205.
[34] Nicas M, Nazaroff WW, Hubbard A. 2005. Toward understanding the risk of secondary airborne infection: emission of respirable pathogens. Journal of Occupational and Environmental Hygiene. 2(3):143-154. doi: 10.1080/15459620590918466.
[35] Kwon SB, Park J, Jang J, Cho Y, Park DS, Kim C, Bae GN, Jang A. 2012. Study on the initial velocity distribution of exhaled air from coughing and speaking," Chemosphere, 87(11):1260-1264. doi: 10.1016/j.chemosphere.2012.01.032.